Marquette University
e-Publications@Marquette

Biomedical Engineering Faculty Research and Publications | Biomedical Engineering, Department of

7-1-2017

Inter-Joint Coordination Deficits Revealed in the Decomposition of Endpoint Jerk During Goal-Directed Arm Movement After Stroke

Jozsef Laczko
University of Pecs

Robert A. Scheidt
Marquette University, robert.scheidt@marquette.edu

Lucia Simo
Northwestern University

Davide Piovesan
Gannon University

Accepted version. *IEEE Transactions on Neural Systems and Rehabilitation Engineering*, Vol. 25, No. 7 (July 2017): 798-810. DOI. © 2017 IEEE. Used with permission.

Marquette University

e-Publications@Marquette

Biomedical Engineering Faculty Research and Publications/ College of Engineering

***This paper is NOT THE PUBLISHED VERSION;* but the author's final, peer-reviewed manuscript.** The published version may be accessed by following the link in the citation below.

IEEE Transactions on Neural Systems and Rehabilitation Engineering, Vol. 25, No. 7 (2017): 798-810. DOI. This article is © IEEE and permission has been granted for this version to appear in e-Publications@Marquette. IEEE does not grant permission for this article to be further copied/distributed or hosted elsewhere without the express permission from IEEE.

Inter-Joint Coordination Deficits Revealed in the Decomposition of Endpoint Jerk During Goal-Directed Arm Movement After Stroke

Jozsef Laczko
University of Pecs and the Wigner Research Centre for Physics, Pecs and Budapest, Hungary
Robert A Scheidt
Department of Biomedical Engineering, Medical College of Wisconsin, Olin Engineering Center, Marquette University, Milwaukee
Lucia S Simo
Physiology, Feinberg School of Medicine, Northwestern University, Chicago, IL
Davide Piovesan
Mechanical and Biomedical Engineering, Gannon University, Erie, PA

Abstract

It is well documented that neurological deficits after stroke can disrupt motor control processes that affect the smoothness of reaching movements. The smoothness of hand trajectories during multi-joint reaching depends on shoulder and elbow joint angular velocities and their successive derivatives as well as on the instantaneous arm configuration and its rate of change. Right-handed survivors of

unilateral hemiparetic stroke and neurologically-intact control participants held the handle of a two-joint robot and made horizontal planar reaching movements. We decomposed endpoint jerk into components related to shoulder and elbow joint angular velocity, acceleration, and jerk. We observed an abnormal decomposition pattern in the most severely impaired stroke survivors consistent with deficits of inter-joint coordination. We then used numerical simulations of reaching movements to test whether the specific pattern of inter-joint coordination deficits observed experimentally could be explained by either a general increase in motor noise related to weakness or by an impaired ability to compensate for multi-joint interaction torque. Simulation results suggest that observed deficits in movement smoothness after stroke more likely reflect an impaired ability to compensate for multi-joint interaction torques rather than the mere presence of elevated motor noise.

Keywords

Impedance modulation, interaction torque, Jacobian, joint stiffness, reach kinematics, rehabilitation robotics

Section I.

Introduction

Stroke survivors with hemiparesis often struggle to perform the simplest of motor tasks, such as reaching and pointing with the paretic arm.[1] In unimpaired individuals, reach hand paths are typically straight with bell-shaped velocity profiles[2] and are commonly modeled as minimizing the integral (with respect to time) of either the squared endpoint jerk represented in extrinsic Cartesian coordinates[3] or the squared angular jerk in intrinsic joint coordinates.[4] By contrast, hemiparetic reaches exhibit systematic misdirection[5] and a lack of hand-path smoothness (1, 6) that can coincide with an increased frequency of terminal corrective submovements.[7] Two neuromotor deficits have been implicated as contributing to the lack of hand trajectory smoothness post-stroke: abnormal management of interaction torques (5, 8; c.f., 9) and an increased variability in the generation of muscle force[10] that is related to muscle weakness.[11] With recovery, hand trajectory smoothness progressively increases;[6,12] this trajectory smoothing corresponds to a gradual reduction in the third time derivative of hand displacement (i.e., hand trajectory jerk) (c.f., 13).

To produce a desired hand trajectory, the nervous system must ultimately coordinate muscle force production with external forces imposed by the environment and with internal forces that arise within the musculoskeletal system itself.[14] Internal forces include those produced by “interaction forces” (i.e., interaction torques) imposed on each limb segment by motion of the segments attached to it.[14] It has been shown previously that shoulder and elbow torques are tightly coordinated in healthy planar reaching movements[15, 16, 17] and 3D arm movements[18] such that interaction torques are well-compensated.[19] Failure of the nervous system to properly compensate for multi-joint interaction torques can lead to increased movement curvature and the desynchronization of motions at the shoulder and elbow joints.[8] After stroke, systematic deficits in the coordination of agonist / antagonist muscle activations arise in some regions of the arm’s workspace due to limitations in the ability of the central nervous system to regulate stretch reflex thresholds in the flexor and extensor muscles in the arm.[20] It is understandable therefore, that abnormal management of interaction torques has been implicated in the degradation of hand path smoothness after stroke.[5, 11] Nevertheless, the mechanistic origin of the control deficit remains the topic of some debate. On the one hand, Beer et al.[5]

hypothesize that changes in movement smoothness post-stroke result from impaired feedforward compensation for the passive interaction torques that arise during multijoint movements (see also 21, 22). On the other hand, Buhrmann and Paolo[23] describe a model of a two-joint arm actuated by antagonistic muscles driven by spinal circuitry that, when properly optimized or "tuned", can compensate for interaction torques without feedforward adjustment of central commands. In this model, central commands are thought to instantiate an open-loop "virtual equilibrium trajectory" comprised of monotonic shifts in specific control signals (λ^{d}) sent to the muscles (see also 23, 24, 25). Although identifying specific control variables is beyond the scope of the current manuscript, errors in specifying the time course and balance of the central commands impinging upon alpha motor neurons (α -MN) and upon the spinal interneurons that modulate α -MN excitability will undoubtedly disrupt the optimal tuning of spinal circuitry, thereby degrading the quality of movement kinematics.[20]

Muscle weakness is another possible contributor to the increased "jerkiness" of reaching movements after stroke. This claim rests on the premise that in order to fully compensate for any given load, weaker muscles require more activation than stronger muscles, and greater voluntary contractions give rise to greater levels of "signal dependent noise", which in healthy subjects manifests as a linear scaling of force variability with respect to the mean force level.[26] Indeed, a study of isometric force production in the paretic-spastic biceps brachii muscle[27] found that greater muscle weakness led to greater variability in the generation of muscle force (i.e., greater motor noise). Increased force production variability has similarly been observed at the wrist and fingers post-stroke.[28, 29] It has been hypothesized that stroke-related increases in neuromotor noise compromises both the planning and execution of movement.[7] In particular, single-unit recordings from muscles in the hemiparetic limb reveal disorderly motor neuron recruitment, which may also contribute to muscle weakness and increased variability of muscle force production.[30] Regardless of its origin, failure to contend with excess motor noise has potential to degrade the accuracy and smoothness of reaching movements post-stroke.

Here, we employ a novel kinematic decomposition analysis[31] to determine the extent to which smoothness of hand movements depends on factors related to the smoothness of contributing joint motions as well as factors related to inter-joint coordination. Guided by results of the decomposition analysis applied to reaching movements performed by small cohorts of stroke survivors and neurologically intact individuals, we use matched forward- and inverse-dynamics simulations to test the competing hypotheses that impairment-related changes in movement smoothness result from improper control of inter-joint interaction torques that normally arise during multi-joint movements or from the presence of excess motor noise. Specifically, hemiparetic stroke survivors and neurologically intact control subjects performed a set of fast, goal-directed reaching movements while holding the handle of a two-joint, horizontal planar robot. We decomposed hand trajectory jerk profiles into components that depend on the first three time derivatives of the shoulder and elbow joint angles as well as on the time derivatives of arm configuration.[31] We then implemented a set of matched inverse- and forward-dynamics computer simulations evaluating the extent to which the pattern of inter-joint coordination deficits expressed by the most impaired stroke survivors can result from each of the two highlighted failure modes of the neural controller: corruption of descending motor commands by uncorrelated noise and failure to account for inter-joint interaction torques that arise during multi-joint planar arm motions. We found that the movement coordination anomalies captured by the jerk decomposition technique could be replicated by neglecting the effect of interaction torque compensation as suggested by,[5] but not merely by increasing motor noise as suggested by.[7]

SECTION II.

Methods

Nineteen human subjects provided written informed consent to participate in this study in compliance with policies established by the Northwestern University Institutional Review Board. Six of the participants were right handed, neurologically intact control subjects (NI; 38–73 years). The remaining thirteen were unilateral, left-hemispheric, hemiparetic stroke survivors (HS: 36–72 years), who self-identified as being right-handed pre-stroke. All HS were in the chronic stage of recovery (>6 months post-stroke) and were recruited from a database of hemiparetic stroke outpatients maintained by the Rehabilitation Institute of Chicago.

All HS participated in an initial evaluation session wherein the same clinician (author LSS) assessed sensorimotor function and impairment with the subject seated in an armless chair (Table I). Clinical assessments included: the sensory and motor portions of the Upper Extremity Fugl-Meyer assessment of physical performance (FM; 32); the modified Ashworth Scale (MAS) assessing abnormal muscle tone at the shoulder, elbow and wrist; and a measure of maximum grip strength. To obtain an overall estimate of spasticity of the upper extremity, the MAS scores were averaged across the joints tested (see also 33). Grip strength was measured using a Jamar Hand Dynamometer with participants seated, their elbow by their side (flexed to a right angle) and with a neutral wrist position. We provided support under the dynamometer during testing, and grip strength was reported as the average of three maximal efforts. Proprioceptive discrimination was evaluated at the shoulder, elbow, wrist, and metacarpophalangeal articulations with the subject's eyes closed using the clinical "*up or down?"* test[34, 35] which is part of the sensory component of the FM. Here, the clinician moves the tested joint up and down several times, and when the joint stops moving, the subject is to indicate joint orientation. Six repetitions were performed at each joint. If response was brisk and accurate (i.e., the subject made no errors), proprioception was rated "intact"; if the subject was unable to respond with confidence (i.e., they made 1 error), proprioception was rated "impaired"; if the subject was unable to determine position (2 or more errors), proprioception was rated "absent". Results of the "*up or down?"* test were confirmed using a robotic test of proprioceptive integrity we have described previously.[36]

TABLE I Clinical Assessments for Stroke Survivors

Age/Sex	Years Post-CVA	FM	MAS	Grip Force* paretic/non-paretic [kg]	Touch	Prop	AMDT
54/F	5	45	0.33	18/36	I: F,W,FA,U	intact	intact†
40/M	6	43	0.66	35/51	N	intact	intact†
69/F	6	41	0	4/25	I: F,W	intact	intact†
60/F	14	28	1.83	8/20	N	intact	intact†
72/F	20	23	1.66	4/25	N	intact	intact†
59/F	5	22	1.66	5/19	N	intact	intact†

CVA: Cerebrovascular Accident; FM: Fugl-Meyer; MAS: Modified Ashworth Score; N: not impaired; I: impaired; F: finger; W: wrist; FA: forearm; U: upper arm; Prop: proprioception; AMDT: Arm Movement Detection Test, a robotic test of arm proprioception, as per [36]; *Normative grip strengths for males in the age range 40-50 years is 47±9.5 kg (mean ± 1 SD). Normative grip strengths for females in the age ranges 50-59, 60-69 and 70+ are 28±6.3 kg, 24±5.3 kg and 20±5.8 kg, respectively [normative values from [68]. †Within normal limits (within the 95% confidence interval of performance) established by a cohort of neurologically intact subjects in [36].

From the HS group, we selected for detailed analysis the group of stroke survivors that retained intact proprioception as measured by both the "*up or down?"* test and robotic assessment; subjects with impaired or absent proprioception were unable to reliably perform the experimental tasks described below in the absence of concurrent visual feedback. All six HS with intact proprioception had Fugl-Meyer motor scores between 20 and 50 (Table I). Three HS participants exhibited moderate motor impairment (FM score >30; HS_{MOD}) whereas the remaining HS participants exhibited severe motor impairment (FM score <30; HS_{SEV}). Participants with severe motor deficits also exhibited moderate levels of arm spasticity as measured with the MAS (Table I). The NI control participants were age and size matched to the selected HS participants.

For the selected stroke survivors, the evaluation session also included a procedure intended to quantify postural bias forces that arise due to hypertonia in the hemiparetic arm (37, 38). Participants were seated comfortably in a high-backed chair fixed in front of a horizontal planar robot (Fig. 1 A). Participants were asked to relax while the robot moved the hand smoothly between sample locations spanning the arm's passive range of motion. The number of sampled positions ranged from 19 to 25. Upon arriving at a desired position, the robot waited 5 s before sampling hand forces to avoid velocity-dependent effects. Sample locations were visited 3 times each in random order. The average hand force vector at each location was plotted and a "posture map" of hypertonic bias forces was interpolated between sample points (Fig. 1B). The integral of this force field with respect to workspace position is the potential energy associated with the passive mechanics of the limb. For each HS, we used their posture map to select a "home" position where bias forces were minimal, and two goal targets: one target (L_{ELBOW}) required movement into a direction of low potential gradient (i.e., within the "low bias force" region); this reach direction required motion predominantly at the elbow in all subjects. The other target (H_{MULTI}) required movement in a direction of high potential gradient (i.e., into the "high bias force" region); this target required considerable motion at both joints. The movement directions cued by the two targets were orthogonal to one another. Active generation of reaches toward both targets would require compensation for substantial interaction torques. Age and size matched NI control participants were to move between the same targets as their matched HS participant.

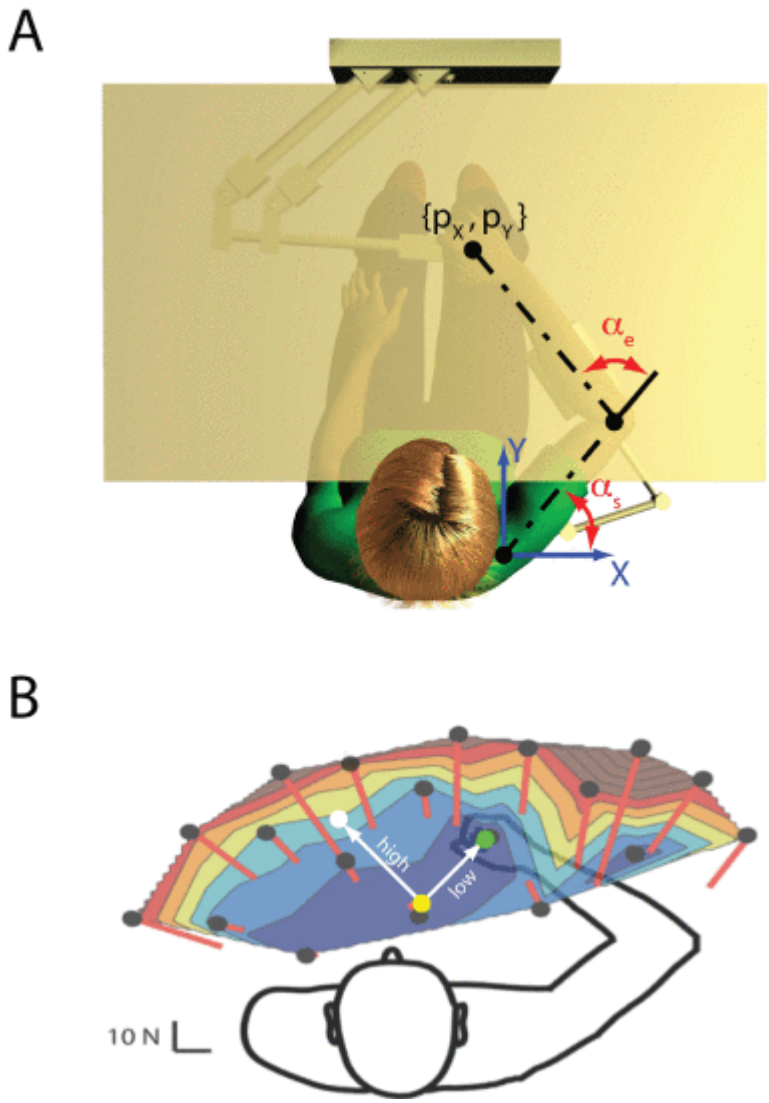

Fig. 1.
A) Experimental setup: $\boldsymbol{\alpha_s}$ **and** $\boldsymbol{\alpha_e}$: joint angular positions measured at the shoulder and elbow joints; $\mathbf{p}_x$, and $\mathbf{p}_y$ **:** endpoint position in a shoulder centered Cartesian {X, Y} coordinate system. B) Representational map of hand forces (red lines) measured at various sample points in the workspace (black dots) and interpolated postural bias forces (color map), reflecting hypertonia in the hemiparetic arm (see text for details). For each stroke survivor, a home target position was selected where bias forces were minimal (yellow target; blue region of the colormap). One goal target was selected such that reaches were performed largely at the elbow and into a direction of relatively low potential gradient (green target). The other target was selected such that reaches required substantial motion at both joints, and were directed into the "high bias force" region of the workspace (white target; yellow region of the colormap). Note that active generation of reaches toward both targets would require compensation for substantial interaction torques.

A. Experimental Protocol

Previous work has shown that movement of the shoulder during unfettered reaching is typically negligible in NI individuals.[39] By contrast, stroke survivors commonly try to use trunk movements to compensate for impaired arm control.[40] To minimize this compensatory strategy, we used a chest

harness to constrain trunk motion such that reaching was performed primarily using rotation of the shoulder and elbow joints.

A light-weight, chair-mounted arm support helped to cancel the effect of gravity and further constrained arm motion to the horizontal plane. The wrist was splinted at 0° flexion and was fixed to the robot's hemi-spherical handle. Participants moved the handle of the robot between targets projected onto an opaque screen 1 cm above the plane of movement using their dominant right hand (NI participants) or their impaired right hand (HS participants). This screen occluded vision of arm, hand, and robot (c.f. 38, 41).

Each subject performed 164 repetitions of a point-to-point reaching task that required moving the hand from a central starting position to one of the two radial targets projected onto the horizontal display screen. In each trial, subjects were to move the robot handle to the goal target and hold it stationary for 1.5 s. The task was performed under two conditions: in the full vision condition (62 trials), a cursor indicating hand position was visible throughout movement; in the "blind" condition (102 trials), there was no feedback of cursor motion during the trial, although the cursor's final position was shown after the end of movement, thus providing knowledge of results. Subjects were instructed: *"When a target appears, look carefully at its location and then capture and hold the target with your cursor as accurately as possible. On some trials you will only see your cursor at the end of your movement. Use this feedback to correct any errors in position."* After each trial, subjects were provided with a visual indicator of peak hand speed and were instructed to maintain it near 0.4 m/s throughout the trial sequence. Real-time cursor feedback was eliminated between trials as the robot returned the hand passively to the start position in anticipation of the next trial. The sequence of trials started with 24 sighted trials (12 to each target) to familiarize subjects with the task, followed by a mixture of 102 blind and 38 sighted trials, which were pseudorandomly distributed in a 3:1 ratio. By including occasional sighted trials in the midst of blind trials, we minimized spatial inaccuracies that can arise due to prolonged absence of visual feedback (42, 43) and also minimized reliance on concurrent visual feedback while generating goal-directed reaching movements. The inter-trial interval was approximately 20 s.

B. Data Analysis

It has been proposed that at least two separate neural control actions contribute to goal-directed arm movements; one is dedicated to the control of arm trajectory whereas another stabilizes limb position in the proximity of spatial targets.[44, 45, 46] In this report, we sought to understand the impact of stroke on the smoothness of movement trajectories. We therefore restricted analysis of each trial to the part of the movement trajectory in which hand speed was higher than 0.1 m/s in order to isolate control action(s) most responsible for reach trajectory.

Partitioning of Endpoint Jerk

The planar velocity of the hand, the endpoint of the 2-joint {shoulder, elbow} kinematic chain, was computed from the time derivatives of the joint angles

$$\boldsymbol{p}'(t) = \boldsymbol{J}(t)\boldsymbol{\alpha}'(t) \qquad (1)$$

where the endpoint position **p**(t) = [p_x (t), p_y (t)] is represented in a shoulder centered Cartesian coordinate system and where x points laterally to the right and y points in the forward direction (see Fig. 1 A). The apex (′) represents the first derivative with respect to time of the endpoint position **p**(t)

and joint angular position $\boldsymbol{\alpha}(t) = [\alpha_s, \alpha_e]$. The subscript "s" refers to the shoulder joint and "e" to elbow joint. $\boldsymbol{J}$ (t) is the Jacobian matrix of the subject's arm, which varies in time as a function of $\boldsymbol{\alpha}(t)$

$$\boldsymbol{J}(t) = \begin{bmatrix} -l_1\sin(\alpha_s) - l_2\sin(\alpha_s + \alpha_e); & -l_2 sin(\alpha_s + \alpha_e) \\ l_1\cos(\alpha_s) + l_2\cos(\alpha_s + \alpha_e) & l_2 cos(\alpha_s + \alpha_e) \end{bmatrix}.$$

Here, the time dependency of joint rotations has been omitted for notational convenience. l is the length of the limb segment, whereas subscripts 1 and 2 refer to the upper-arm and forearm-plus-hand segments, respectively. Differentiation of (1), with respect to time yields the endpoint acceleration

$$\mathbf{p}''(\mathrm{t}) = \mathbf{J}'(\mathrm{t})\boldsymbol{\alpha}'(\mathrm{t}) + \mathbf{J}(\mathrm{t})\boldsymbol{\alpha}''(\mathrm{t}).$$

Differentiating a second time yields an equation for endpoint jerk, an instantaneous measure of movement smoothness, represented as a sum of three components[47]

$$\mathbf{p}'''(\mathrm{t}) = \mathbf{J}''(\mathrm{t})\boldsymbol{\alpha}'(\mathrm{t}) + 2\mathbf{J}'(\mathrm{t})\boldsymbol{\alpha}''(\mathrm{t}) + \mathbf{J}(\mathrm{t})\boldsymbol{\alpha}'''(\mathrm{t}). \quad (2)$$

For convenience, we denote the three terms of the right-hand side of (2), as

$$\begin{aligned} \boldsymbol{G_1}(t) &= \boldsymbol{J}''(t)\boldsymbol{\alpha}'(t); \\ \boldsymbol{G_2}(t) &= 2\boldsymbol{J}'(t)\boldsymbol{\alpha}''(t); \\ \boldsymbol{G_3}(t) &= \boldsymbol{J}(t)\boldsymbol{\alpha}'''(t). \end{aligned}$$

Taking the square of both sides of (2) and integrating over time yields a scalar measure of hand trajectory smoothness

$$\begin{aligned} \int_{t1}^{t2} \mathbf{p}'''(\mathrm{t})^2 \mathrm{dt} = \quad & \int_{t1}^{t2} |\mathrm{G}_{\mathbf{1}}(\mathrm{t})|^2 \mathrm{dt} + \int_{t1}^{t2} |\mathrm{G}_{\mathbf{2}}(\mathrm{t})|^2 \mathrm{dt} \\ & + \int_{t1}^{t2} |\mathrm{G}_{\mathbf{3}}(\mathrm{t})|^2 \mathrm{dt} + \int_{t1}^{t2} \mathbf{G}_{\mathbf{MIXED}}(\mathrm{t})\, \mathrm{dt}, \end{aligned} \quad (3)$$

where

$$\begin{aligned} \int_{t1}^{t2} \mathbf{G}_{\mathbf{MIXED}}(\mathrm{t})\mathrm{dt} = \quad 2 \int_{t1}^{t2} (& < \mathbf{G_1}(\mathrm{t}), \mathbf{G_2}(\mathrm{t}) > \\ & + < \mathbf{G_1}(\mathrm{t}), \mathbf{G_3}(\mathrm{t}) > \\ & + < \mathbf{G_2}(\mathrm{t}), \mathbf{G_3}(\mathrm{t}) >) \mathrm{dt} \end{aligned}$$

and where <, > denotes the inner product, | .| is the vector norm, whereas t1 and t2 are the start and end times of the movement (defined here as the time interval during which hand speed was continuously higher than 0.1 m/s). In this way, we partition the integral of the square of the total endpoint jerk into four components. Each of the first three integrals on the right side of (3) depends purely on one of the components of the right side of (2). We refer to the fourth term on the right side of (3) as the "mixed term", because it depends on a mixture of the three components on the right side of (2).

Component $\mathbf{G_3}$ describes the contributions of angular jerk at the shoulder and elbow joints to endpoint jerk, distinct from the contributions of joint angular velocities, accelerations and any change of arm configuration. By contrast, the other two terms ($\mathbf{G_1}$ and $\mathbf{G_2}$) both depend on joint angular velocity *and* acceleration, but not on joint angular jerk. This dependence on velocity and acceleration is both explicit

(in terms of dependence on $\alpha'$and α'') and implicit due to time differentiation of the Jacobian. When determining which component or components contribute most to the total endpoint jerk, it is important to note that the first three terms on the right side of (3) are positive because they are integrals of squared functions, whereas the fourth term can take on negative values if the angles between the vector components on the right side of (2) are greater than 90°. The angle between the different jerk components is a composite performance measure that reflects the degree of spatiotemporal coordination between displacements, velocities and accelerations at the shoulder and elbow joints.

For example, from the definition of the inner product of continuous signals

$$\langle \mathrm{G}_i(t), \mathrm{G}_j(t) \rangle = \int_{-\infty}^{+\infty} \mathbf{G}_i(t) \cdot \mathbf{G}_j(t) dt$$

Where $i, j \in \{1,2,3\}$, and from the definition of the correlation function

$$R_{ij}(\tau) = \int_{-\infty}^{+\infty} \mathbf{G}_i(t) \cdot \mathbf{G}_j(t+\tau) dt = \langle \mathrm{G}_i(t), \mathrm{G}_j(t+\tau) \rangle$$

we recognize equivalence when the time lag τ between the signals is taken to be zero. Thus, a negative scalar product between $\mathbf{G}_i(t)$ and $\mathbf{G}_j(t)$ implies a negative value of the correlation function, as can occur for similar phasic signals that are in counter-phase due to temporal shift (e.g., two sine waves of the same frequency shifted relative to one another by more than a quarter cycle, i.e., >90°), or for dissimilar signals that are nearly synchronous but inherently counter-phase (e.g., sine and cosine waveforms with the cosine signal trailing slightly in time).

Simulation of Endpoint Trajectories

We performed a series of numerical simulations to test the competing hypotheses that changes in movement smoothness post-stroke result from improper control of inter-joint interaction torques that normally arise during multi-joint movements or due to the presence of excess motor noise related to weakness. We simulated reaches in the two experimental directions for each participant. The simulated reach endpoints lay on the perimeter of a semicircle that was centered on the home position. In all cases, the simulated home position was placed relative to the shoulder joint at the actual location used in the experiment performed with the robot. The radius of the semicircle was calculated as the average distance between the home position and the two experimental reach targets.

To assess the sensitivity of simulation results to various fundamental assumptions, simulations evaluated two different kinematic descriptions of "ideal" endpoint motion and eight different ways of estimating limb segment inertial parameters. Specifically, planar movements were modeled using the minimum jerk (MJ) time profile[3, 48] and the sigmoidal (SG) time profile.[49] Limb segment parameters for each subject were estimated using each of the following estimation methods: Hanavan (HV);[50] Dempster (DE);[51] Chandler (CH);[52] Clauser (CL);[53] McConville (MC);[54] Zatsiorsky and Seluyanov (Z1);[55] Zatsiorsky (Z2);[56] and de Leva (DL).[57] A detailed comparison between the eight inertial parameter estimation methods can be found in.[39] Inverse kinematics analyses were used to compute shoulder and elbow joint angle time series, while inverse dynamics computations were used to compute the corresponding joint torque time series during each simulated reach.

For the minimum jerk kinematic model, the main parameters characterizing the hand trajectory time series are the hand's initial and final positions, as well as the total duration of the movement assuming that the hand starts and stops at rest. We matched the simulations to the across-subject average reach duration, which was approximately 0.6 s. According to this model, peak hand speed is determined by movement distance and will therefore be lower for subjects with shorter reaches. By contrast, the sigmoidal trajectory model allows for the specification of maximum speed independent of movement duration of the reach. By imposing the same trial duration of 0.6 s, a parameter was adjusted to limit maximum hand speed to 0.4 m/s for all simulated reaches.

When considering rigid motion of a two-joint arm supported in the horizontal plane, the torques about the joints can be represented by the dynamic equation

$$\boldsymbol{M}(\boldsymbol{\alpha})\ddot{\boldsymbol{\alpha}} + \boldsymbol{H}(\boldsymbol{\alpha}, \dot{\boldsymbol{\alpha}}) = \boldsymbol{\tau} \qquad (4)$$

Where $\boldsymbol{\alpha}$ is the vector of joint angles, and $\boldsymbol{\tau}$ is the vector of joint torques. The inertial and Coriolis matrices $\boldsymbol{M}(\boldsymbol{\alpha})and\boldsymbol{H}(\boldsymbol{\alpha}, \dot{\boldsymbol{\alpha}})$ are in the form[39]

$$\begin{aligned} \boldsymbol{M}(\boldsymbol{\alpha}) &= \begin{bmatrix} \kappa + 2\beta c_e & \chi + \beta c_e \\ \chi + \beta c_e & \chi \end{bmatrix}; \\ \boldsymbol{H}\left(\boldsymbol{\alpha}, \dot{\boldsymbol{\alpha}}\right) &= \begin{bmatrix} -\beta s_e \dot{\alpha}_e & \chi - \beta s_e \left(\dot{\alpha}_e + \dot{\alpha}_s\right) \\ \beta s_e \dot{\alpha}_s & 0 \end{bmatrix} \end{aligned} \qquad (5)$$

where

$$\begin{aligned} \kappa &= I_{zs} + I_{ze} + m_s r_s^2 + m_e(l_s^2 + r_e^2) \\ \beta &= m_e l_s r_e \\ \chi &= I_{ze} + m_e r_e^2. \end{aligned} \qquad (6)$$

Here, as before, the subscript "s" refers to variables of the upper-arm link and shoulder joint, while "e" identifies variables of the forearm-hand link and elbow joint. l is the segmental link length; m is segmental mass, r is the distance between the link center of mass and the proximal joint, and the I_z parameters are the moments of inertia about the z-axis orthogonal to the plane of movement, calculated at the link's center of mass. We use simplified notation for trigonometric functions with $s_e = \sin(\alpha_e)$ and $C_e = \cos(\alpha_e)$

Simulating Neuromotor Control Deficits

Given the 16 different permutations of kinematic and anthropometric models, (4) was used to estimate the joint torques necessary to obtain the specified endpoint trajectories. Forward dynamics simulations were then performed to study consequences of two potential motor control deficits: 1) failing to account for shoulder-elbow interaction torques, and 2) degradation of descending motor commands through the addition of motor noise. Note that (4) describes the mechanics of our experimental task; the simulations make no assumptions as to either the control variables driving the movement or the underlying source of coordination deficits contributing to a lack of movement smoothness in the hemiparetic arm. For each distinct subject model and for each target, we simulated all possible combinations of control deficits wherein: 1) interaction torque compensation was either normal (full feedforward compensation for interaction torques), moderately impaired (feedforward

compensation for inter-joint interaction torques 15% lower than the theoretical ideal values) or severely impaired (feedforward compensation 45% lower than the theoretical ideal) (c.f., 5); and 2) joint torque production was either uncorrupted by signal-dependent noise (with a signal-to-noise ratio SNR $= \infty$; an unrealistic best case scenario), corrupted by motor noise in the normal physiological range (1% of the RMS torque,[58] which corresponds to a SNR of 40 dB), and a range of pathological SNRs ranging from 30 dB down to 10 dB (where the strength of the noise signal is approximately 1/3 that of the signal).

Specifically, we simulate the effect of additional motor noise under the assumption that input torques could be corrupted with band limited noise with maximum frequency of 7 Hz,[39] with a signal to noise ratio defined as[48]

$$SNR = 20\log_{10}\frac{\sqrt{\frac{1}{T}\int_0^T[\boldsymbol{\tau}(t)]^2dt}}{\sqrt{\frac{1}{T}\int_0^T[\boldsymbol{\tau}(t)\cdot\gamma\cdot\boldsymbol{\eta}(t)]^2dt}}$$

where $\boldsymbol{\tau}(t)$ is the vector of joint torques, $\boldsymbol{\eta}(t)$ is a zero mean, band-limited random signal with unit root mean square magnitude, and γ is a scaling factor used to set specific desired SNR values. Because the torques required to drive the hand through each planned trajectory depend on the limb segment inertial parameters, simulations driven by each ideal trajectory were repeated using each of the eight inertial models for each subject. Using eight different sets of inertial and Coriolis matrices derived from the various published estimation approaches allowed us to determine the effect of degraded neuromotor control within the uncertainty inherent to limb segment inertial estimation.

C. Statistical Hypothesis Testing

We used the simulations to test the competing hypotheses that changes in movement smoothness post-stroke result from improper control of inter-joint interaction torques that normally arise during multi-joint movements[5] or from excess motor noise.[7] The simulations were guided by experimentally-measured reach kinematics, which we analyzed using a non-parametric inverse-normal-transform (INT; 59) Rank Transformation test (RT Type 1; 60) applied to selected structural components of the endpoint jerk. In the INT-RT1 test, the entire set of observations for a given dependent variable is first ranked from smallest to largest, with the smallest observation having rank 1, the second smallest rank 2, and so on (average ranks are assigned in case of ties). Next, ranks are standardized by computing their normal or z-scored ranking

$$INT = \Phi^{-1}\left(\frac{R_i}{(n+1)}\right)$$

where R_i are the ranks of the dependent variable, n is the number of observations and Φ^{-1} is the inverse normal transformation. Finally, a parametric F test (mixed model repeated measures ANOVA) is applied to the INT standardized ranks. The INT-RT1 analysis takes advantage of both between and within block information, resulting in a distribution-free test that compares favorably with the Friedman test and Fischer's randomization test in terms of robustness and power (59, 60), and has also been shown to be acceptable for assessing interactions (60). We used INT-RT1 to test the main effects of impairment level {severe, mild, control}, trial type {sighted, blind}, and movement direction

$\{L_{ELBOW}, H_{MIXED}\}$ on each integral of the squared jerk component derived from the experimental data.

We then analyzed the ability of simulated reach kinematics to replicate key features of the human subject data by performing repeated measures analysis of variance (RM-ANOVA) on each integral of the squared jerk component derived from each of the 5760 simulated reaches. We tested the effect of simulated deficits in compensation for interaction torques {no deficit, 15% reduction, 45% reduction}, increasing levels of signal-dependent motor noise {no noise (SNR $= \infty$), "normal" noise (SNR = 40 dB), and three levels of enhanced noise: 30 dB, 20 dB, 10 dB}, and movement direction $\{L_{ELBOW}, H_{MULTI}\}$ within each group of simulated trajectories {minimum jerk or sigmoidal}. Post-hoc, Tukey honest significance difference (HSD) analysis was performed to compare—across simulations using all eight of the body segmental parameter models—the effect of motor-noise and failure to compensate for inter-joint interaction torques versus trajectories obtained without simulated impairment. Across all analyses, effects were considered significant at the family-wise error rate of $\alpha = 0.05$.

SECTION III.

Results

Movement Kinematics–Experiment

Fig. 2 presents representative hand trajectories obtained experimentally from a HS participant (Fig. 2, top) and a NI control subject (Fig. 2, bottom) for trajectories made to a target requiring movement into a high bias force region of the workspace and primarily shoulder + elbow joint rotations (left: H_{MULTI}) and a target requiring movement within the low bias force region and primarily elbow joint rotation (right: L_{ELBOW}). The experimental trajectories conform to the expectation that reaching movements of stroke survivors are less smooth than those made by neurologically intact control subjects in that they follow paths that exhibit greater curvature and more terminal inflections.

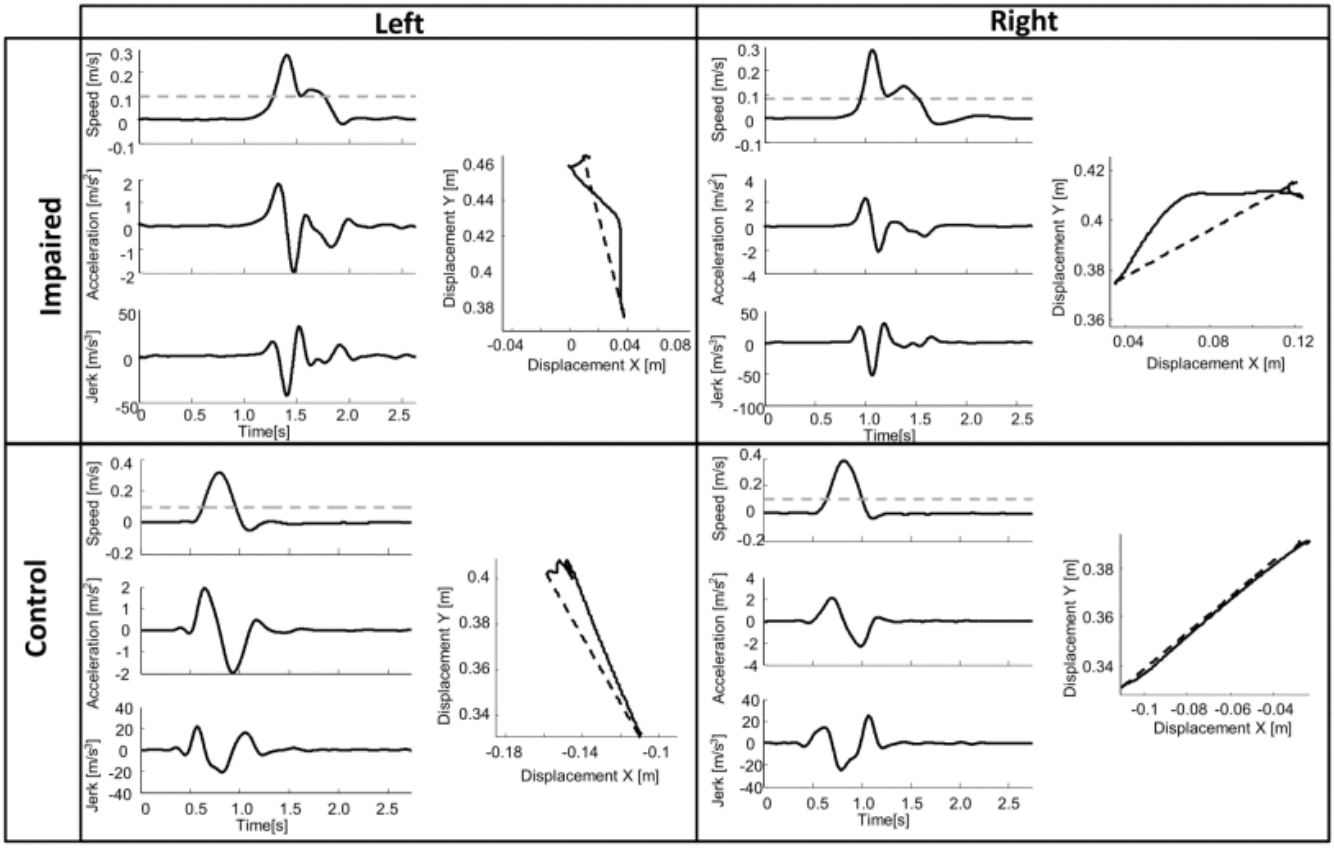

Fig. 2.
Representative hand trajectories and tangential speed, acceleration and jerk profiles from a selected stroke survivor (top) and NI control participant (bottom) for movements made to targets requiring approximately equal amounts of shoulder and elbow joint motion (left) and primarily elbow motion (right). In the trajectory plots, dashed lines represent the ideal straight-line hand path between home and goal targets.

Fig. 3 presents a decomposition of the x- and y-axis components of total endpoint jerk into the three joint angular time series $\boldsymbol{G_1}, \boldsymbol{G_2}$ and $\boldsymbol{G_3}$ for representative trials from a stroke survivor (top) and a control subject (bottom). For all participants and both movement directions, total endpoint jerk throughout the entire movement was dominated by $\boldsymbol{G_3}(t)$, the component of (2) related to angular jerk at the shoulder and elbow joints. Based on this outcome, one might expect that the right-hand terms involving $\boldsymbol{G_3}$ (i.e., $|\boldsymbol{G_3}(\mathrm{t})|^2$ and the "mixed term" involving $< \mathbf{G_1}(\mathrm{t}), \mathbf{G_3}(\mathrm{t}) >$ and $< \mathbf{G_2}(\mathrm{t}), \mathbf{G_3}(\mathrm{t}) >$) should contribute most importantly to the scalar measure of hand path smoothness defined by (3).

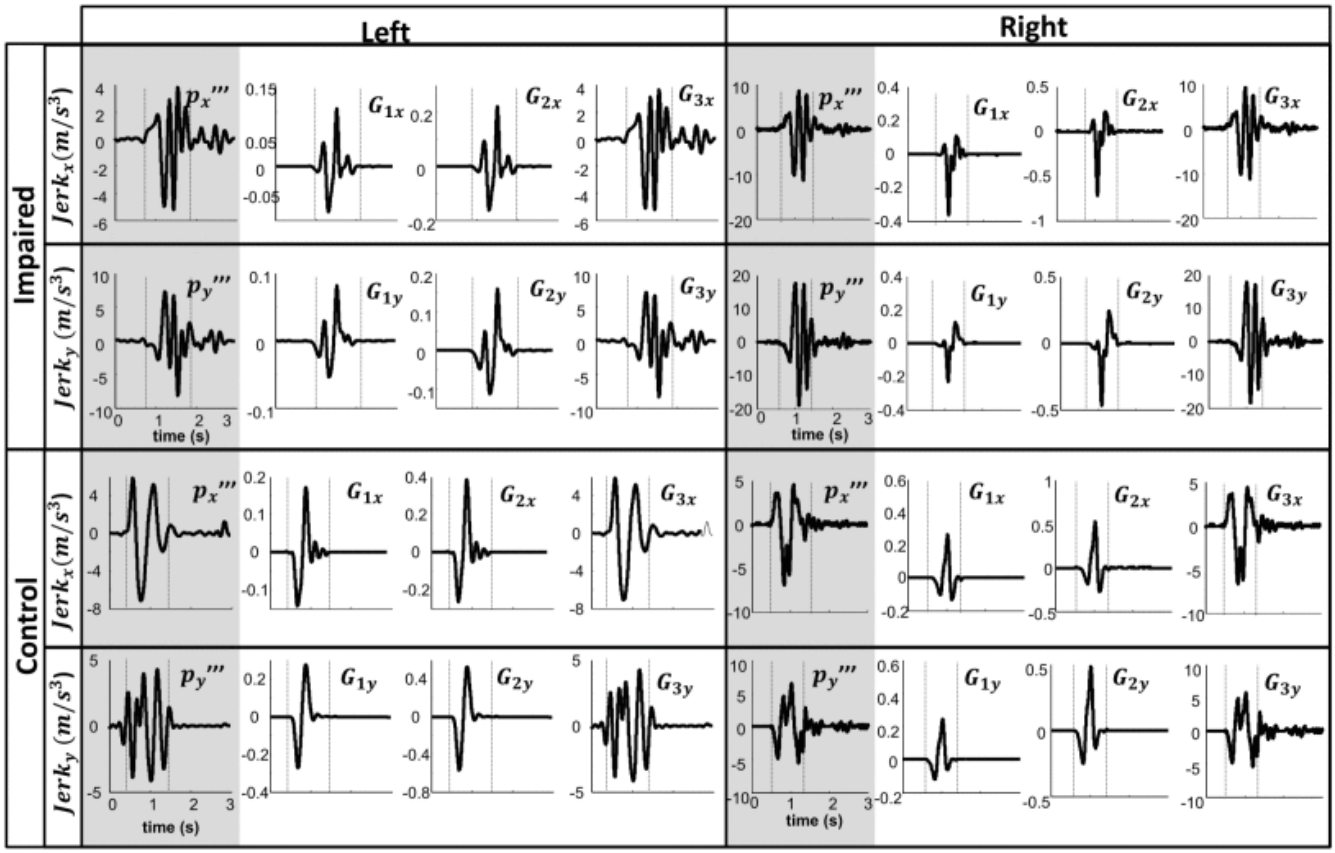

Fig. 3.
Cartesian components of the total endpoint jerk (shaded plots) and the corresponding structural components for representative reaching movements (as in Fig. 2) from two selected participants (HS: top; NI: bottom). Note the different scales for each component. The third component (G_3 (t)) dominates the total jerk $p'''(t)$) in all cases. The contribution of the first and second structural components are very small.

Indeed, across all participant groups, visual feedback conditions, and movement directions, contribution of the first and second terms (G_1, G_2) to the integral of the squared total jerk was very small (under 5%), whereas the component $\int \mathbf{G_3}(t)^2$ explained nearly 100% of the total endpoint jerk (Fig. 4).

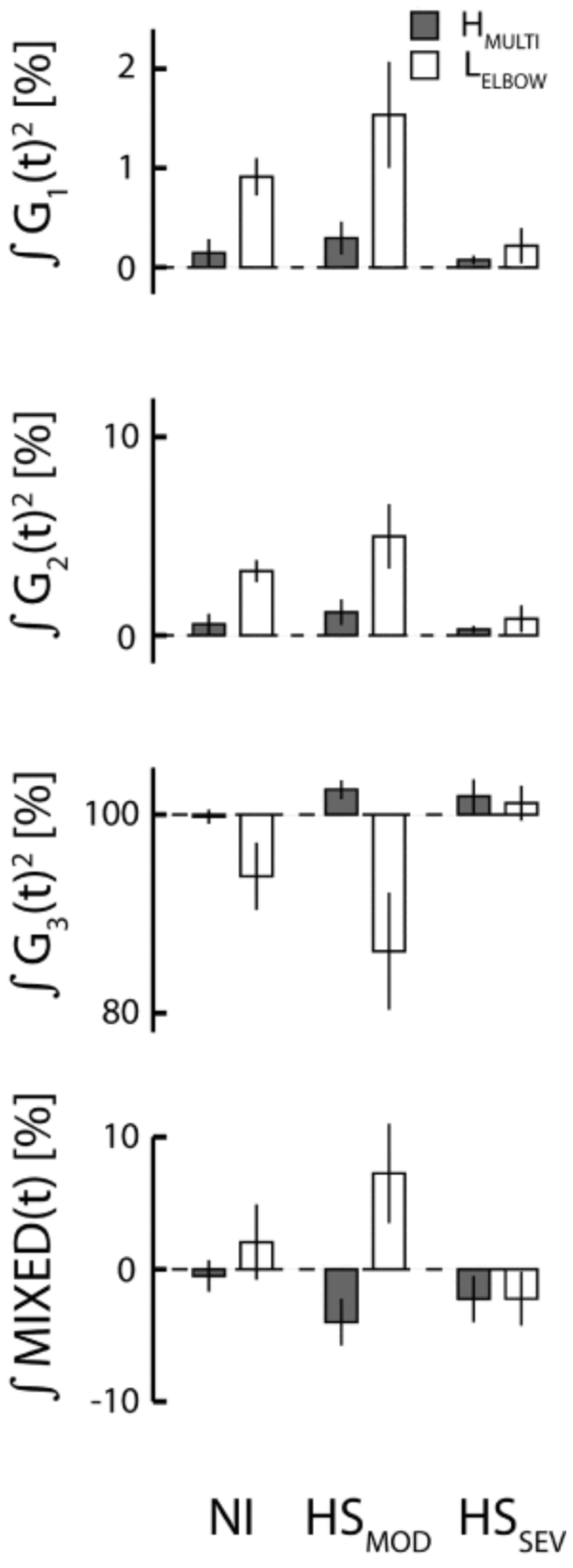

Fig. 4.
Population statistics for each structural component as a function of movement direction in each participant group. Shaded bars: multi-joint reaches into a region of the workspace with high bias forces; open bars: reaches within a region of low bias force using primarily elbow extension. To create these plots, jerk component values

were collapsed (averaged) across trials and visual feedback conditions within each subject and movement direction because there were no discernable differences in any parameter between trials wherein the cursor was visible versus those where it was not.

For all structural components of endpoint jerk, non-parametric INT-RT1 analysis found significant main effects of impairment group [$F_{(2,27)} > 5.77$; p <0.024 in all four cases] and reach direction [$F_{(1,27)} > 38.59$; p <0.0005], and a significant interaction between these two factors [$F_{(2,27)} > 5.00$; p <0.014]. We observed no main effect of visual feedback condition [$F_{(1,27)} < 0.91$; p > 0.349], or any interaction between this term and the others [$F_{(1or2,27)} > 0.58$; p <0.453]. With regards to the interaction between impairment group and movement direction, NI and HS_{MOD} subjects had higher $\int \mathbf{G_1}(t)^2$ and $\int \mathbf{G_2}(t)^2$ contributions (and lower $\int \mathbf{G_3}(t)^2$ contributions) for movements to the L_{ELBOW} target than movements to the H_{MULTI} movements (Fig. 4). HS_{SEV} did not exhibit this pattern of behavior. Surprisingly, across feedback conditions, we found the component $\int \mathbf{G_3}(t)^2$ to be higher than 100% for all HS reaches to the H_{MULTI} targets, and also for the L_{ELBOW} reaches made by the severely impaired individuals. This is possible because the mixed term $\int \mathbf{G_{MIXED}}(t)$of the cost function was negative for these participants.

To confirm this supposition, we performed a set of Wilcoxon signed ranks analyses – within each subject and movement direction — to ascertain whether $\int \mathbf{G_{MIXED}}(t)$was indeed negative for many HS reaches. For this analysis, we set the within condition criterion threshold for significance to p = 0.05. We found that for all six HS participants, reaches into the H_{MULTI} direction had negative $\int \mathbf{G_{MIXED}}(t)$ components whereas the NI subjects had values that did not differ systematically from 0. By contrast, NI and HS_{MOD} participants exhibited positive $\int \mathbf{G_{MIXED}}(t)$ components when reaching into the L_{ELBOW} direction, whereas two of the three HS_{SEV} exhibited negative $\int \mathbf{G_{MIXED}}(t)$ values (the third subject's values did not differ from zero). To summarize, decomposition of endpoint jerk into individual and mixed joint components reveals a pattern of abnormalities in the coordination of multi-joint reaching post-stroke. When motions at the two joints are well synchronized, as in NI participants, the angles between the individual jerk time series {$\boldsymbol{G}$**1**,$\boldsymbol{G}$**2**} and $\boldsymbol{G}$**3** are less than 90°, yielding a mixed term that is not different from zero or slightly positive. The negative mixed term observed during reaching in the H_{MULTI} target in HS_{MOD} subjects and in both directions for the HS_{SEV} subjects indicates that at least one angle between jerk components $\boldsymbol{G_1}$, $\boldsymbol{G_2}$, and $\boldsymbol{G_3}$ was larger than 90° in these cases.

Because the Jacobian of the arm varies smoothly and slowly as a function of hand position within the reachable workspace, the most likely factor contributing to the negative mixed term within any given reach is a disorganization of the temporal coordination between motions at the shoulder and elbow joints (such as that which might arise from an inability to compensate for inter-joint interaction torques that normally arise during multi-joint movements; c.f. 5).

Movement Kinematics–Simulation

We performed a series of paired, inverse- and forward-dynamic simulations to test the competing hypotheses that the presence of substantial motor noise or deficits in the ability to compensate for inter-joint interaction torques give rise to the particular pattern of inter-joint coordination deficits observed during our experimental testing. Specifically, we simulated the planning of straight, horizontal planar hand trajectories to L_{ELBOW} and H_{MULTI} targets using two different descriptions of the "ideal" hand trajectory. We then performed inverse dynamics analyses to estimate the joint torques required to drive the limb through the desired trajectories. Because the inverse dynamics

calculations depend on accurate estimates of limb segment inertial parameters and because the literature describes several different ways to estimate these parameters, we repeated the analysis using eight different estimation approaches gleaned from the literature. Finally, we simulated impaired neural control in two ways. First, we compromised simulated descending motor commands by adding motor noise to the joint torques driving the forward dynamic simulations based on the ideal plans. We also simulated impaired inter-joint coordination by decreasing the magnitude of interaction torque contributions to the simulated resultant joint torques.

Initial MANOVA examining the effects of impairment group, anthropometric model, trajectory model, direction, and noise level on the four structural components of endpoint jerk ($\int \mathbf{G_1}(t)^2$, $\int \mathbf{G_2}(t)^2$, $\int \mathbf{G_3}(t)^2$, and $\int \mathbf{G_{MIXED}}(t)$) found no main effect of anthropometric model on these dependent variables, but main effects of the remaining independent factors. We therefore averaged across anthropometric models prior to conducting follow-on analyses. We also found that when simulating "unimpaired" trajectories with the "ideal" polynomial (minimum jerk) and sigmoidal models, only the sigmoidal model yielded $\int \mathbf{G_{MIXED}}(t)$ terms approximating magnitudes observed experimentally; whereas $\int \mathbf{G_{MIXED}}(t)$ averaged −1.48±1.42% for the sigmoidal model, $\int \mathbf{G_{MIXED}}(t)$ averaged −12.54±3.46 for the polynomial model—an order of magnitude larger than expected. Consequently, we only consider the sigmoidal model in the following analyses of the impact of simulated motor deficits on movement smoothness.

Separate repeated measures ANOVA for the subject-specific simulations found, for each of the four components of endpoint jerk, main effects of simulated motor noise [$F_{(4,319)} > 17.94$, p <0.0005], main effects of simulated impairment in the compensation for inertial torques [$F_{(2,319)} > 15.48$, p <0.0005], and interactions between the two factors [$F_{(2,319)} > 38.98$, p <0.0005]. By contrast, we observed no main effect of impairment group [$F_{(2,319)} < 4.09$, p >0.216], no main effect of movement direction [$F_{(1,319)} < 2.00$, p >0.632], nor interaction between movement direction and any other factor [$F_{(2or4,319)} < 1.65$, p >0.644].

Fig. 5 presents how the values of each jerk component responds to corruption of the shoulder and elbow joint torques during forward dynamic simulation. As in the experimental trajectories, contribution from $\int \mathbf{G_1}(t)^2$ and $\int \mathbf{G_2}(t)^2$ to the integral of the squared total jerk was very small (well under 5%), whereas the component $\int \mathbf{G_3}(t)^2$ explained slightly more than 100% of the total endpoint jerk performance value. The magnitude of $\int \mathbf{G_{MIXED}}(t)$ was smallest in the absence of corruption and in the presence of low amounts of simulated motor noise. Regardless of noise level, the (negative) magnitude of the mixed term increased as the model's compensation for inter-joint interaction torques was degraded. This pattern paralleled the pattern of results presented in Fig. 4, where the magnitude of the mixed term was largest in the most impaired reaches. The main effects of noise level and the interaction between noise and deficits of interaction torque compensation appear to be due to a compounding of effects at the very highest levels of both factors.

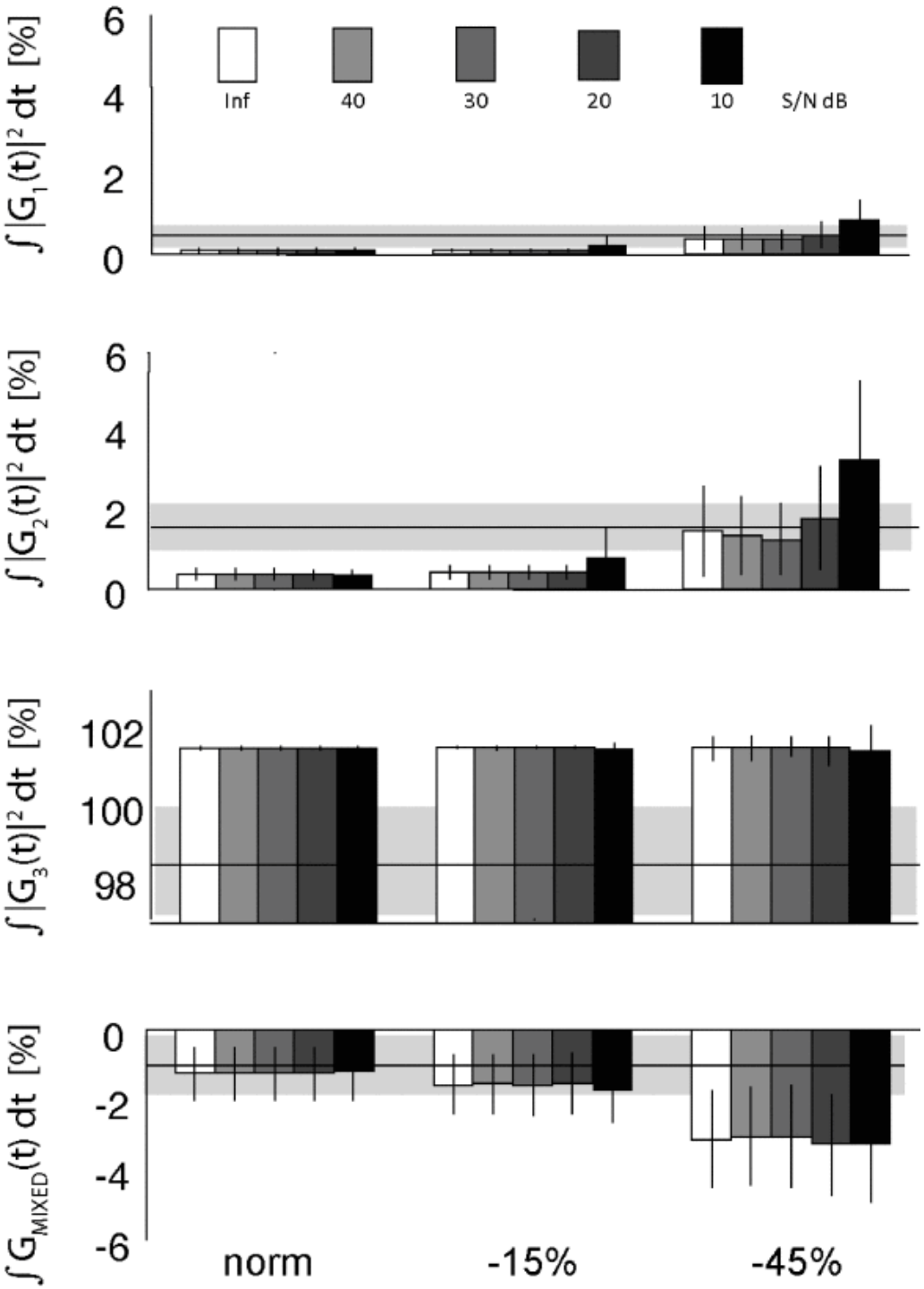

Fig. 5.
Signed magnitudes of the structural components of total endpoint jerk derived from paired forward- and inverse-dynamic simulations of reaching movements performed with different amounts of failure to account for interaction torques and differing amounts of control signal noise. Left column: norm = full interaction torque compensation; Middle column: 85% compensation; Right column: 55% compensation. Noise levels ranged from no noise (signal to noise ratio S/R = ∞ ; best case scenario) to S/R values of 40 dB, 30 dB, 20 dB, and 10 dB (bar color code in top panel). Horizontal lines and shading: mean ±1 SD values observed experimentally from NI control participant reaches toward the H_{MULTI} target.

It is interesting to note that neither set of "ideal" endpoint trajectories replicated the precise numerical pattern of $\int \mathbf{G_3}(\mathrm{t})^2$ and mixed term values revealed in our experimental data. The observed values from the NI control subjects for each structural component are presented in Fig. 5 as horizontal lines and shading representing ±1 SD. When minimum-jerk movements were simulated as in,[3] values of $\int \mathbf{G_3}(\mathrm{t})^2$ greatly exceeded the squared integral of the total endpoint jerk and the mixed term component of (3) was negative and large for all simulated impairment levels. In fact, the magnitude of the negative mixed term was 5–10 times larger than the values derived from experimentally measured trajectories across all participant groups. By contrast, the sigmoidal hand displacement function yielded magnitudes of the $\int \mathbf{G_3}(\mathrm{t})^2$ and mixed terms that more closely approximated values obtained experimentally.

Nevertheless, and despite experimentally-observed reach trajectories deviating from theoretically ideal trajectories, the pattern of increasing magnitude of the (negative) mixed term with increasing inability to compensate for interaction torques—but not increased motor noise in isolation—support the hypothesis [5] that post-stroke deficits of movement smoothness derive—at least in part—from deficits in compensation for interaction torques that arise during multi-joint reaching movements.

SECTION IV.

Discussion

This paper describes a novel analysis of hand kinematics during horizontal planar reaching movements performed by stroke survivors and unimpaired control participants. Endpoint jerk was decomposed into terms that depend upon shoulder- and elbow-joint angular velocity, angular acceleration and angular jerk via the arm's Jacobian matrix and its first two time derivatives (c.f., 44). We determined which terms in the decomposition dominate the description of endpoint motion and how each term's contribution to the total endpoint jerk varied with increasing motor impairment post-stroke. For all participants, we found that endpoint jerk was dominated by the product of the arm's Jacobian and the vector of joint angular jerk (i.e., the joint-based component $\boldsymbol{G_3}$), thus demonstrating that the smoothness of endpoint motion is largely determined by the smoothness of the individual joint trajectories (c.f. 31). This finding suggests that the most effective way for the central nervous system to maximize hand trajectory smoothness is to minimize $\boldsymbol{G_3}$, the component of endpoint jerk dependent on joint angular jerk. Surprisingly, for severely-impaired stroke survivors, the integral with respect to time of $\boldsymbol{G_3}$ squared ($\int \boldsymbol{G_3}(\mathrm{t})^2$) was larger than the integral of the square of the endpoint jerk itself ($\int \dddot{p}(\mathrm{t})^2$) , thus becoming overdominant. This can only happen when the angle between two different components in (2) grows larger than 90° (i.e., when the "mixed' component $\int \mathbf{G_{MIXED}}(\mathrm{t})$ in (3) becomes negative). The most likely factor contributing to the negative mixed term is a disorganization of the spatiotemporal coordination between shoulder and elbow joint motions, as might arise from an inability to pre-plan and compensate for inter-joint interaction torques.[5]

To investigate this possibility, we implemented a set of matched inverse- and forward-dynamics computer simulations evaluating the extent to which the pattern of inter-joint coordination deficits post-stroke can result from two failure modes of the neural controller: corruption of descending motor commands by uncorrelated noise and failure to account for inter-joint interaction torques that arise during multi-joint planar arm motions. In particular, we investigated the relative contributions of the

component terms of (3) to the overall hand trajectory smoothness using two different "ideal" hand trajectoies: a fifth order "minimum jerk" polynomial and a sigmoidal time-profile of the hand trajectory. For each ideal endpoint trajectory, we simulated impaired post-stroke control in several ways: 1) with varying degrees of motor impairment caused by discounting a percentage of ideal compensation for interaction torques, as suggested in 5; 2) with varying degrees of impairment caused by adding execution noise as suggested by 7; and 3) the combination of these factors. Importantly, we found that a signature of impaired performance—the (negative) magnitude of $\int \mathbf{G_{MIXED}}(\mathrm{t})$ —increased in magnitude as we progressively degraded the model's ability to predict and compensate for inter-joint interaction torques, but not when we only added motor noise to the forward dynamic joint torques. These simulation results lend support to the hypothesis that a deficit of inter-joint coordination—impaired ability to compensate for inter-joint interaction torques—contributes importantly to post-stroke movement deficits.

Of the two ideal hand trajectories, the sigmoidal trajectory provided a much better match to the experimental data than did the minimum jerk trajectory. Whereas mimum jerk trajectories yielded $\int \boldsymbol{G_3}(\mathrm{t})^2$ estimates that grossly exceeded the total endpoint jerk and yielded large negative mixed terms in all simulated conditions, the sigmoidal hand displacement model yielded mixed term component values that came to approximate the experimental values observed in the most severely-impaired stroke survivors, as the percentage of uncompensated interaction torques increased. It is unclear why simulated minimum jerk hand trajectories yielded $\int \boldsymbol{G_3}(\mathrm{t})^2$ and mixed term values that overestimated experimental values. One possibility is that real-world movements fail to conform to certain aspects of the simple minimum jerk trajectory, such as ideally-straight hand paths, perfectly symmetric velocity profiles, and so on (c.f., 1). Moreover, while it has been previously demonstrated that a minimum jerk hand trajectory does not necessarily yield a minimum jerk trajectory in joint space,[61] other computational issues pertaining to the numerical simulations might also be considered, such as differences in estimating the numerical derivatives of polynomial functions vs. exponential functions.[62]

Although we attempted to constrain our analysis such that we focused largely on the initial, feedforward portion of reach trajectories, it is in fact possible that stroke-related deficits in feedback control (c.f., 63) could contribute to deficits of movement smoothness, because anomalous feedback of spinal and/or long-loop origin might partially confound otherwise intact descending motor commands (48; see also 23). Anomalous reflexes can also alter the apparent endpoint stiffness of the limb.[64, 65] This could cause deficits in multi-joint coordination if, as suggested by,[66] the CNS normally solves the problem of controlling the limbs using a passive motion paradigm wherein the elastic energy at the joints is regulated via modulation of joint stiffness $\boldsymbol{K}_{\alpha}(\boldsymbol{\alpha}, \boldsymbol{u})$ (see also 8). In this case, joint stiffness K is a function of both the limb's position in joint space $\boldsymbol{\alpha}$ and the activations $\boldsymbol{u}$ of mono- and bi-articular muscles, all of which are functions of time. Previous work[67] has demonstrated that an integrable pseudo-inverse of the Jacobian in the form

$$\boldsymbol{J}_K^{\#} = \boldsymbol{K}_{\alpha}^{-1}\boldsymbol{J}^T(\boldsymbol{J}\boldsymbol{K}_{\alpha}^{-1}\boldsymbol{J}^T)^{-1} \qquad (7)$$

gives a unique solution to the inverse kinematic problem of redundant robots. (7) is a form of generalized inverse where $\boldsymbol{K}_{\alpha}^{-1}$ enters as a quadratic form "weighting matrix". The matrix $\boldsymbol{J}_K^{\#}$ can be inverted using basic linear algebra techniques to obtain a Jacobian that is a function of the joint stiffness matrix

$$\boldsymbol{J}_K = (\boldsymbol{J}\boldsymbol{K}_{\alpha}^{-1}\boldsymbol{J}^T)\left(\boldsymbol{J}^{T^{-1}}\boldsymbol{K}_{\alpha}\right). \qquad (8)$$

It is immediate to see that by substituting (8) into (2), the derivatives of the Jacobian matrix with respect to time (e.g., G_1 and G_2) are functions of the change in joint stiffness. Therefore, it is possible that the variations in jerk components we observed experimentally might also be explained in part by an abnormal modulation of joint stiffness, which is often observed in stroke survivors.[65] Future studies should investigate the role of volitional control of joint stiffness in the modulation of endpoint jerk, how such control may be compromised throughout the workspace post-stroke by spasticity and other deficits of neuromuscular control, and the extent to which impaired control of joint stiffness can degrade the ability to compensate for inter-joint interaction torques that normally arise during multi-joint movements.

Our study has a number of limitations. The first pertains to sample size; although our sample of stroke survivors was rather small, the primary goal of this manuscript was to demonstrate—through simulation—the ability of the jerk decomposition analysis to capture a curious and salient feature of movement kinematics observed in all tested movements made by the most severely impaired individuals and in the most challenging movements made by moderately impaired participants—namely, the possibility of negative $\int \mathbf{G_{MIXED}}(\mathrm{t})$ contributions to the overall endpoint jerk. Future studies involving a larger number of stroke survivors should both confirm the effects reported here and examine the specific effects of rehabilitation procedures on improving smoothness of motions at the individual joints as well as on improving inter-joint coordination. Another limitation was the inability of our "ideal" simulations—those performed without simulated impairments—to account for the precise numerical results of the decomposition applied to the NI participant reaches (i.e., discrepancy between the simulated results for components $\int \boldsymbol{G_1}(\mathrm{t})^2$, $\int \boldsymbol{G_2}(\mathrm{t})^2$, $\int \boldsymbol{G_3}(\mathrm{t})^2$ and the average NI performance depicted by the horizontal lines and confidence bound estimates in Fig. 5). Moreover, none of our simulations generated the relatively large positive $\int \mathbf{G_{MIXED}}(\mathrm{t})$ component generated during $\mathrm{L_{ELBOW}}$ movements by the moderately impaired $\mathrm{HS_{MOD}}$ participants. We have attempted a variety of manipulations of the ideal trajectories such as allowing for varying degrees of skew in the velocity profile (data not shown) but have been unable to attain a perfect match across all decomposition components of endpoint jerk. This remains an open question for future simulation work. Despite these limitations, we believe the endpoint jerk decomposition analysis presented here to be a valuable tool that can determine the extent to which the smoothness of hand movement depends on the smoothness of motions at the various joints as distinct from factors related to inter-joint coordination. By doing so, the analysis provides additional kinematic variables that can be used as informative outcome measures for clinical studies concerned with movement coordination.

*****.Normative grip strengths for males in the age range 40–50 years is 47±9.5 kg (mean ± 1SD). Normative grip strengths for females in the age ranges 50–59, 60–69 and 70+ are 28±6.3 kg, 24±5.3 kg and 20±5.8 kg, respectively [normative values from.[68]

†.Within normal limits (within the 95% confidence interval of performance) established by a cohort of neurologically intact subjects in.[36]

References

1. D. G. Kamper, A. N. McKenna-Cole, L. E. Kahn, D. J. Reinkensmeyer, "Alterations in reaching after stroke and their relation to movement direction and impairment severity", *Arch. Phys. Med. Rehabil.*, vol. 83, no. 5, pp. 702-707, May 2002.
2. P. Morasso, "Spatial control of arm movements", *Experim. Brain Res.*, vol. 42, no. 2, pp. 223-227, 1981.
3. T. Flash, N. Hogan, "The coordination of arm movements: An experimentally confirmed mathematical model", *J. Neurosci.*, vol. 5, no. 7, pp. 1688-1703, Jul. 1985.
4. T. Flash, J. Winters, S. Y. Woo, "The organization of human arm trajectory control" in Biomechanics and Movement Organization, New York, NY, USA:Springer, pp. 282-301, 1990.
5. R. F. Beer, J. P. A. Dewald, W. Z. Rymer, "Deficits in the coordination of multijoint arm movements in patients with hemiparesis: Evidence for disturbed control of limb dynamics", *Experim. Brain Res.*, vol. 131, no. 3, pp. 305-319, 2000.
6. B. Rohrer et al., "Movement smoothness changes during stroke recovery", *J. Neurosci.*, vol. 22, no. 18, pp. 8297-8304, Sep. 2002.
7. P. H. McCrea, J. J. Eng, "Consequences of increased neuromotor noise for reaching movements in persons with stroke", *Experim. Brain Res.*, vol. 162, no. 1, pp. 70-77, 2005.
8. W. Wang, T. Johnson, R. L. Sainburg, N. Dounskaia, "Interlimb differences of directional biases for stroke production", *Experim. Brain Res.*, vol. 216, no. 2, pp. 263-274, 2012.
9. M. F. Levin, "Interjoint coordination during pointing movements is disrupted in spastic hemiparesis", *Brain*, vol. 119, no. 1, pp. 281-293, 1996.
10. N. Lodha, G. Misra, S. A. Coombes, E. A. Christou, J. H. Cauraugh, H. James, "Increased force variability in chronic stroke: Contributions of force modulation below 1 Hz", *PLoS ONE*, vol. 8, pp. e83468, Dec. 2013.
11. H. Topka, J. Konczak, K. Schneider, A. Boose, J. Dichgans, "Multijoint arm movements in cerebellar ataxia: Abnormal control of movement dynamics", *Experim. Brain Res.*, vol. 119, no. 4, pp. 493-503, 1998.
12. H. I. Krebs, N. Hogan, M. L. Aisen, B. T. Volpe, "Robot-aided neurorehabilitation", *IEEE Trans. Rehabil. Eng.*, vol. 6, no. 1, pp. 75-87, Mar. 1998.
13. W. L. Nelson, "Physical principles for economies of skilled movements", *Biol. Cybern.*, vol. 46, no. 2, pp. 135-147, 1983.
14. R. L. Sainburg, C. Ghez, D. Kalakanis, "Intersegmental dynamics are controlled by sequential anticipatory error correction and postural mechanisms", *J. Neurophysiol.*, vol. 81, no. 3, pp. 1045-1056, 1999.
15. G. L. Gottlieb, Q. Song, G. L. Almeida, D. A. Hong, D. D. Corcos, "Directional control of planar human arm movement", *J. Neurophysiol.*, vol. 78, no. 6, pp. 2985-2998, 1997.
16. R. L. Sainburg, M. F. Ghilardi, H. Poizner, C. Ghez, "Control of limb dynamics in normal subjects and patients without proprioception", *J. Neurophysiol.*, vol. 73, no. 2, pp. 820-835, Feb. 1995.
17. C. Ghez, R. Sainburg, "Proprioceptive control of interjoint coordination", *Can. J. Physiol. Pharmacol.*, vol. 73, no. 2, pp. 273-284, 1993.
18. R. Tibold, J. Laczko, "The effect of load on torques in point-to-point arm movements: A 3D model", *J. Motor Behavior*, vol. 44, no. 5, pp. 341-350, 2012.
19. P. Pigeon, S. B. Bortolami, P. DiZio, J. R. Lackner, "Coordinated turn-and-reach movements. II. Planning in an external frame of reference", *J. Neurophysiol.*, vol. 89, no. 1, pp. 290-303, 2003.

20. N. K. Musampa, P. A. Mathieu, M. F. Levin, "Relationship between stretch reflex thresholds and voluntary arm muscle activation in patients with spasticity", *Experim. Brain Res.*, vol. 181, no. 4, pp. 579-593, 2007.
21. Y. Uno, M. Kawato, R. Suzuki, "Formation and control of optimal trajectory in human multijoint arm movement", *Biol. Cybern.*, vol. 61, no. 2, pp. 89-101, 1989.
22. R. Osu, D. W. Franklin, H. Kato, H. Gomi, K. Domen, T. Yoshioka, M. Kawato, "Short- and long-term changes in joint co-contraction associated with motor learning as revealed from surface EMG", *J. Neurophysiol.*, vol. 88, pp. 991-1004, Aug. 2002.
23. T. Buhrmann, E. A. Di Paolo, "Spinal circuits can accommodate interaction torques during multijoint limb movements", *Front. Comput. Neurosci.*, vol. 8, pp. 144, Nov. 2014.
24. A. G. Feldman, M. F. Levin, "The origin and use of positional frames of reference in motor control", *Behav. Brain Sci.*, vol. 18, no. 4, pp. 723-806, 1995.
25. P. L. Gribbel, D. J. Ostry, "Compensation for loads during arm movements using equilibrium-point control", *Experim. Brain Res.*, vol. 135, no. 4, pp. 474-482, 2000.
26. K. E. Jones, A. F. Hamilton, D. M. Wolpert, "Sources of signal-dependent noise during isometric force production", *J. Neurophysiol.*, vol. 88, no. 3, pp. 1533-1544, 2002.
27. S. H. Chang, G. E. Francisco, P. Zhou, W. Z. Rymer, S. Li, "Spasticity weakness force variability and sustained spontaneous motor unit discharges of resting spastic-paretic biceps brachii muscles in chronic stroke", *Muscle Nerve*, vol. 48, no. 1, pp. 85-92, 2013.
28. N. Lodha, S. K. Naik, S. A. Coombes, J. H. Cauraugh, "Force control and degree of motor impairments in chronic stroke", *Clin. Neurophysiol.*, vol. 121, no. 11, pp. 1952-1961, 2010.
29. N. Lodha, G. Misra, S. A. Coombes, E. Christou, J. H. Cauraugh, H. James, "Increased force variability in chronic stroke: Contributions of force modulation below 1 Hz", *PLoS ONE*, vol. 8, no. 12, pp. e83468, 2013.
30. J. J. Gemperline, S. Allen, D. Walk, W. Z. Rymer, "Characteristics of motor unit discharge in subjects with hemiparesis", *Muscle Nerve*, vol. 18, no. 10, pp. 1101-1114, 1995.
31. J. Laczko, S. Jaric, J. Tihanyi, V. M. Zatsiorsky, M. L. Latash, "Components of the end-effector jerk during voluntary arm movements", *J. Appl. Biomech.*, vol. 16, no. 1, pp. 14-25, Feb. 2000.
32. A. R. Fugl-Meyer, L. Jääskö, I. I. Leyman, S. Olsson, S. Steglind, "The post-stroke hemiplegic patient. 1. A method for evaluation of physical performance", *Scandin. J. Rehabil. Med.*, vol. 7, no. 1, pp. 13-31, 1975.
33. K. M. Zackowski, A. W. Dromerick, S. A. Sahrmann, W. T. Thach, A. J. Bastian, "How do strength sensation spasticity and joint individuation relate to the reaching deficits of people with chronic hemiparesis?", *Brain*, vol. 12, no. 5, pp. 1035-1046, 2004.
34. E. L. DeGowin, R. L. DeGowin, Customers Who Viewed Degowin & Degowin's Diagnostic Examination Also Viewed, New York, NY, USA:Collier-Macmillian, 1987.
35. O. Epstein, G. Perkin, J. Cookson, D. D. Bono, Clinical Examination, London, U.K.:Mosby, 2004.
36. L. Simo, L. Botzer, C. Ghez, R. A. Scheidt, "A robotic test of proprioception within the hemiparetic arm post-stroke", *J. Neuroeng. Rehabil.*, vol. 11, pp. 77, Apr. 2014.
37. P. Kanade, C. Ghez, R. A. Scheidt, "Spatial mapping of posture-dependent endpoint forces in the hypertonic arm post-stroke: A novel application of rehabilitation robotics", *Proc. Neural Control Movement Soc.*, 2008.
38. L. S. Simo, L. S. D. Piovesan, L. Botzer, M. Bengtson, C. P. Ghez, R. A. Scheidt, "Arm kinematics during blind and visually guided movements in hemiparetic stroke survivors", *Soc. Neurosci.*, 2013.

39. D. Piovesan, A. Pierobon, P. DiZio, J. R. Lackner, "Comparative analysis of methods for estimating arm segment parameters and joint torques from inverse dynamics", *J. Biomech. Eng.*, vol. 133, no. 3, pp. 031003, 2011.
40. M. F. Levin, S. M. Michaelsen, C. M. Cirstea, A. Roby-Brami, "Use of the trunk for reaching targets placed within and beyond the reach in adult hemiparesis", *Experim. Brain Res.*, vol. 143, no. 2, pp. 171-180, 2002.
41. L. S. Simo, D. Piovesan, J. Laczko, C. Ghez, R. Scheidt, "Submovements during reaching movements after stroke", *Proc. Eng. Med. Biol. Soc. (EMBC)*, pp. 5357-5360, Aug. 2014.
42. J. P. Wann, S. F. Ibrahim, "Does limb proprioception drift?", *Experim. Brain Res.*, vol. 91, no. 1, pp. 162-166, 1992.
43. R. A. Scheidt, M. A. Conditt, E. L. Secco, F. A. Mussa-Ivaldi, "Interaction of visual and proprioceptive feedback during adaptation of human reaching movements", *J. Neurophysiol.*, vol. 93, no. 6, pp. 3200-3213, 2005.
44. R. S. Woodworth, "The accuracy of voluntary movement", *Psychol. Rev.*, vol. 3, pp. 1-119, Jul. 1899.
45. D. Elliott, S. Hansen, L. E. M. Grierson, J. Lyons, S. J. Bennett, S. J. Hayes, "Goal-directed aiming: Two components but multiple processes", *Psychol. Bull.*, vol. 136, no. 6, pp. 1023-1044, Nov. 2010.
46. R. A. Scheidt, C. Ghez, "Separate adaptive mechanisms for controlling trajectory and final position in reaching", *J. Neurophysiol.*, vol. 98, no. 6, pp. 3600-3613, 2007.
47. V. Zatsiorsky, "Kinematics of human motion" in Human Kinetics, Champaign, IL, USA:, 1997.
48. D. Piovesan, M. Casadio, F. A. Mussa-Ivaldi, P. Morasso, "Comparing two computational mechanisms for explaining functional recovery in robot-therapy of stroke survivors", *Proc. 4th IEEE RAS EMBS Int. Conf. Biomed. Robot. Biomechatronics (BioRob)*, pp. 1488-1493, Jun. 2012.
49. D. Piovesan, A. Pierobon, P. P. DiZio, J. R. Lackner, "Measuring multi-joint stiffness during single movements: Numerical validation of a novel time-frequency approach", *PLoS ONE*, vol. 7, pp. e33086, Mar. 2012.
50. E. P. J. Hanavan, "A mathematical model of the human body", 1964.
51. W. T. Dempster, "Space requirements of the seated operator. Geometrical kinematic and mechanical aspects of the body with special reference to the limbs", 1955.
52. R. F. Chandler, C. E. Clauser, J. T. McConville, H. M. Reynolds, J. W. Young, "Investigation of inertial properties of the human body", 1975.
53. C. E. Clauser, J. T. McConville, J. W. Young, "Weight volume and center of mass of segments of the human body", 1969.
54. J. T. McConville, T. D. Churchill, I. Kaleps, C. E. Clauser, J. Cuzzi, "Anthropometric relationships of body and body segment moments of inertia", 1980.
55. V. Zatsiorsky, V. Seluyanov, H. Matsui, "The mass and inertia characteristics of the main segments of the human body 30" in Human Kinetics, Champaign, IL, USA:, pp. 1152-1159, 1983.
56. V. M. Zatsiorsky, V. M. Zatsiorsky, "Best predictive regression equations for estimating inertial properties of body segments in males" in Human Kinetics, Champain, IL, USA:, pp. 600-601, 2002.
57. P. de Leva, "Adjustments to Zatsiorsky–Seluyanov's segment inertia parameters", *J. Biomechan.*, vol. 29, no. 9, pp. 1223-1230, 1996.
58. C. M. Harris, D. M. Wolpert, "Signal-dependent noise determines motor planning", *Nature*, vol. 394, pp. 780-784, Aug. 1998.
59. H. Luepsen, "Comparison of nonparametric analysis of variance methods a Monte Carlo study: Part A: Between subjects designs—A vote for van der Waerden" in Regionales Rechenzentrum, Cologne, Germany:, Aug. 2016.

60. W. J. Conover, R. Iman, "Rank transformations as a bridge between parametric and nonparametric statistics", *Amer. Statist.*, vol. 35, no. 3, pp. 124-129, 1981.
61. T. Okadome, M. Honda, "Kinematic construction of the trajectory of sequential arm movements", *Biological*, vol. 80, no. 3, pp. 157-169, 1999.
62. A. A. Giunta, L. T. Watson, J. Koehler, "A comparison of approximation modeling techniques: Polynomial versus interpolating models", *Amer. Inst. Aeronautics Astron.*, vol. 4758, pp. 1-14, Jan. 1998.
63. N. J. O'Dwyer, L. Ada, "Reflex hyperexcitability and muscle contracture in relation to spastic hypertonia", *Curr. Opinion Neurol.*, vol. 9, no. 6, pp. 451-455, 1996.
64. M. M. Mirbagheri, X. Niu, D. Varoqui, "Prediction of stroke motor recovery using reflex stiffness measures at one month", *IEEE Trans. Neural Syst. Rehabil. Eng.*, vol. 20, no. 6, pp. 762-770, Nov. 2012.
65. D. Piovesan, P. Morasso, P. Giannoni, M. Casadio, "Arm stiffness during assisted movement after stroke: The influence of visual feedback and training", *IEEE Trans. Neural Syst. Rehabil. Eng.*, vol. 21, no. 3, pp. 454-465, May 2013.
66. F. Mussa-Ivaldi, P. Morasso, R. Zaccaria, "Kinematic networks. A distributed model for representing and regularizing motor redundancy", *Biological*, vol. 60, no. 1, pp. 1-16, 1988.
67. F. A. Mussa-Ivaldi, N. Hogan, "Integrable solutions of kinematic redundancy via impedance control", *Int. J. Robot. Res.*, vol. 10, no. 5, pp. 481-491, Oct. 1991.
68. N. M. Massy-Westropp, T. K. Gill, A. W. Taylor, R. W. Bohannon, C. Hill, "Hand grip strength: Age and gender stratified normative data in a population-based study", *Biomed. Res. Notes*, vol. 4, pp. 127, Apr. 2011.